SUPPLEMENTARY FIGURES:

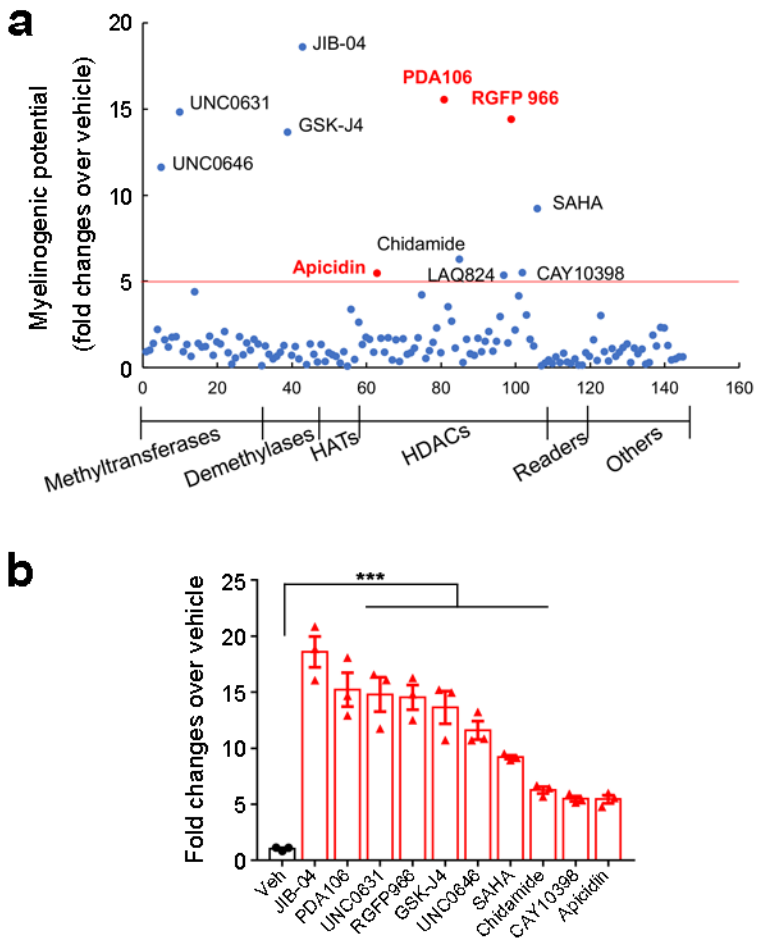

Supplementary Figure 1. Effects of small-molecule epigenetic enzymatic inhibitors on *Egr2* expression. (**a**) Expression of *Egr2* was assessed in SCs treated with a library of epigenetic drugs. Each point represents a single compound, with *Egr2* expression compared to Veh. The red line indicates upregulation of *Egr2* by more than 5-fold. The inhibitors that preferentially target HDAC3 were labeled as red. (**b**) qPCR quantification of *Egr2* expression in SCs treated with eleven compounds that upregulated *Egr2* by more than 5-fold. (Data are presented as mean ± s.e.m.; $n = 3$ independent experiments; two-tailed unpaired Student's *t*-test; $P_{\text{Veh versus JIB-04}} = 0.0002$, $t_{\text{Veh versus JIB-04}} = 12.67$, d.f. = 4; $P_{\text{Veh versus PDA106}} = 0.0007$, $t_{\text{Veh versus PDA106}} = 9.365$, d.f. = 4; $P_{\text{Veh versus UNC0631}} = 0.0009$, $t_{\text{Veh versus UNC0631}} = 8.974$, d.f. = 4; $P_{\text{Veh versus RGFP966}} = 0.0003$, $t_{\text{Veh versus RGFP966}} = 12.25$, d.f. = 4; $P_{\text{Veh versus GSK-J4}} = 0.001$, $t_{\text{Veh versus GSK-J4}} = 8.633$, d.f. = 4; $P_{\text{Veh versus UNC0646}} = 0.0002$, $t_{\text{Veh versus UNC0646}} = 12.85$, d.f. = 4; $P_{\text{Veh versus SAHA}} < 0.0001$, $t_{\text{Veh versus SAHA}} = 40.71$, d.f. = 4; $P_{\text{Veh versus Chidamide}} < 0.0001$, $t_{\text{Veh versus Chidamide}} = 16.55$, d.f. = 4; $P_{\text{Veh versus CAY10398}} < 0.0001$, $t_{\text{Veh versus CAY10398}} = 17.2$, d.f. = 4; $P_{\text{Veh versus Apicidin}} = 0.0003$, $t_{\text{Veh versus Apicidin}} = 11.71$, d.f. = 4). ***$P < 0.001$.

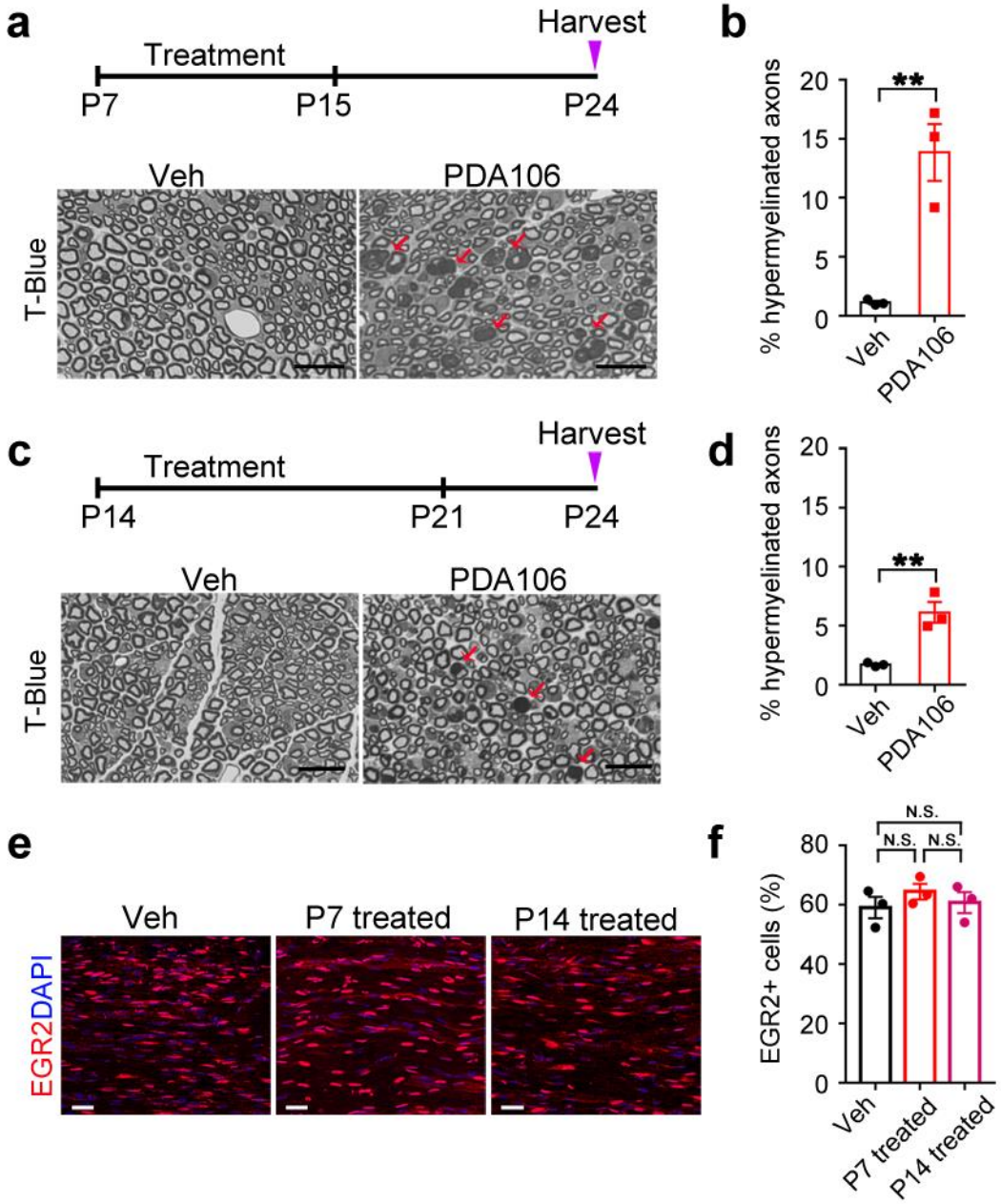

Supplementary Figure 2. Effects of pharmacological inhibition of HDAC3 on myelination at different stages. (**a**) Upper: Schematic diagram showing drug treatment scheme. Mice were treated with Veh or PDA106 from P7 to P15. Sciatic nerves were harvested at P24. Bottom: Representative toluidine blue-stained images of cross sections of sciatic nerves from Veh- and PDA106-treated mice. Arrow indicates hypermyelinated axons. n = 3 animals/group, with 5 images for each mouse. Scale bars: 20 μm. (**b**) Quantification of hypermyelinated axons in sciatic nerves from Veh- and PDA106-treated mice at P24. (Data are presented as mean ± s.e.m.; n = 3 animals/group; two-tailed unpaired Student's t-test; P = 0.0061, t = 5.228, d.f. = 4). (**c**) Upper: Schematic diagram showing drug treatment scheme. Mice were treated with Veh or PDA106 from P14 to P21. Sciatic nerves were harvested at P24. Bottom: Representative toluidine blue-stained images of cross sections of sciatic nerves from Veh- and PDA106-treated mice. Arrow indicates hypermyelinated axons. n = 3

animals/group, with 5 images for each mouse. Scale bars: 20 µm. (**d**) Quantification of hypermyelinated axons in sciatic nerves from Veh- and PDA106-treated mice at P24. (Data are presented as mean ± s.e.m.; n = 3 animals/group; two-tailed unpaired Student's t-test; P = 0.0073, t = 5.027, d.f. = 4). (**e**) Representative images of longitudinal cryosections of sciatic nerves from Veh- and P7 or P14 started PDA106-treated mice. Immunostaining was performed at P24 with EGR2 (red) and DAPI (blue). n = 3 animals/group, with 5 images for each mouse. Scale bar: 20 µm. (**f**) Quantifications at P24 of $EGR2^+$ cells in sciatic nerves from Veh- and P7 or P14 started PDA106-treated mice. (Data are presented as mean ± s.e.m.; n = 3 animals/group; one-way ANOVA with Tukey's multiple comparisons test; $F_{(2, 6)}$ = 0.697, $P_{\text{Veh versus P7 treated}}$ = 0.5197, $P_{\text{Veh versus P14 treated}}$ = 0.9323, $P_{\text{P7 treated versus P14 treated}}$ = 0.7196). n.s., not significant. $^{**}P < 0.01$.

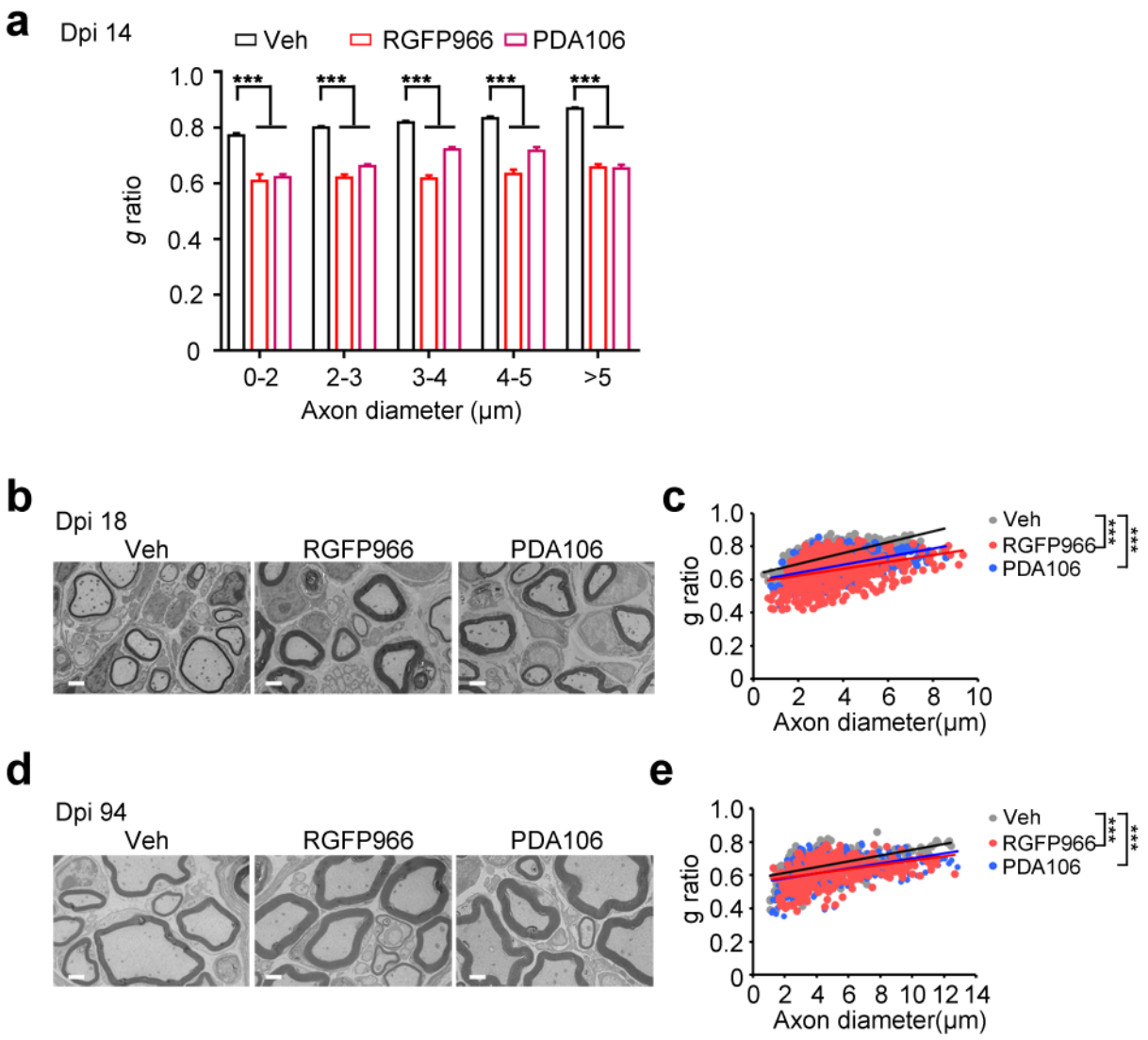

Supplementary Figure 3. Effects of pharmacological inhibition of HDAC3 on remyelination. (**a**) Quantification of *g* ratios of groups of axons with the indicated diameters at Dpi 14. (Data are presented as mean ± s.e.m.; *n* = 3 animals/group; one-way ANOVA with Tukey's multiple comparisons test; 0 - 2 µm, $F_{(2, 114)} = 59.91$, $P_{\text{Veh versus RGFP966}} < 0.0001$, $P_{\text{Veh versus PDA106}} < 0.0001$; 2 - 3 µm, $F_{(2, 337)} = 137.8$, $P_{\text{Veh versus RGFP966}} < 0.0001$, $P_{\text{Veh versus PDA106}} < 0.0001$; 3 - 4 µm, $F_{(2, 227)} = 89.09$, $P_{\text{Veh versus RGFP966}} < 0.0001$, $P_{\text{Veh versus PDA106}} < 0.0001$; 4 - 5 µm, $F_{(2, 122)} = 31.72$, $P_{\text{Veh versus RGFP966}} < 0.0001$, $P_{\text{Veh versus PDA106}} < 0.0001$; > 5 µm, $F_{(2, 82)} = 47.03$, $P_{\text{Veh versus RGFP966}} < 0.0001$, $P_{\text{Veh versus PDA106}} < 0.0001$). (**b**) Representative electron micrographs of regenerated sciatic nerve cross sections from Veh- and HDAC3 inhibitors-treated mice at Dpi 18. *n* = 3 animals/group, with 5 images for each mouse. Scale bars: 2 µm. (**c**) Quantification of *g* ratios of the axons of regenerated sciatic nerves from Veh- and HDAC3 inhibitors-treated mice at Dpi 18. (Data are presented as mean ± s.e.m.; *n* = 408 axons from 3 control mice, 574 axons from 3 RGFP966 treated mice and 546 axons from 3 PDA106 treated mice; one-way ANOVA with Tukey's multiple comparisons test; $F_{(2, 1525)} = 153$, $P_{\text{Veh versus RGFP966}} < 0.0001$, $P_{\text{Veh versus PDA106}} < 0.0001$). (**d**) Representative electron micrographs of regenerated sciatic nerve cross sections from Veh- and HDAC3 inhibitors-treated

mice at Dpi 94. n = 3 animals/group, with 5 images for each mouse. Scale bars: 2 µm. (**e**) Quantification of g ratios of the axons of regenerated sciatic nerves from Veh- and HDAC3 inhibitors-treated mice at Dpi 94. (Data are presented as mean ± s.e.m.; n = 407 axons from 3 control mice, 364 axons from 3 RGFP966 treated mice and 436 axons from 3 PDA106 treated mice; one-way ANOVA with Tukey's multiple comparisons test; $F_{(2,\ 1201)} = 26.69$, $P_{\text{Veh versus RGFP966}} < 0.0001$, $P_{\text{Veh versus PDA106}} < 0.0001$). ***$P < 0.001$.

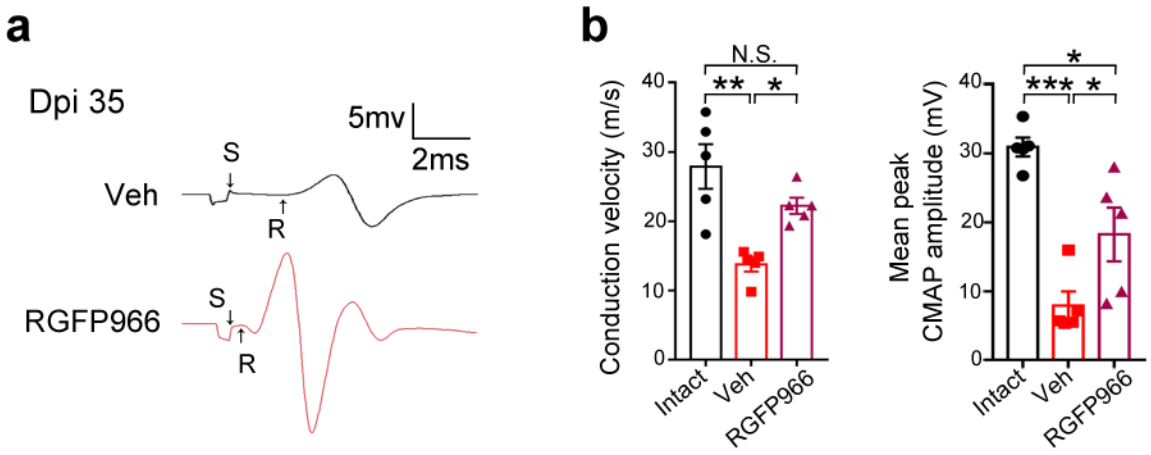

Supplementary Figure 4. HDAC3 inhibitor treatment enhances functional recovery after sciatic nerve transection. (**a**) Representative recordings of CMAPs of regenerated sciatic nerves at Dpi 35 from Veh- and RGFP966-treated mice (S, stimulus; R, initiation of CMAP response). n = 5 animals/group. (**b**) Quantification of the conduction velocity and mean peak of CMAP amplitude of injured sciatic nerves from Veh- and RGFP966-treated mice. (Data are presented as mean ± s.e.m.; n.s., not significant; n = 5 animals/group; one-way ANOVA with Tukey's multiple comparisons test; conduction velocity, $F_{(2, 12)} = 11.88$, $P_{\text{Intact versus Veh}} = 0.0011$, $P_{\text{Intact versus RGFP966}} = 0.1697$, $P_{\text{Veh versus RGFP966}} = 0.0331$; mean peak of CMAP amplitude, $F_{(2, 12)} = 18.77$, $P_{\text{Intact versus Veh}} = 0.0001$, $P_{\text{Intact versus RGFP966}} = 0.0142$, $P_{\text{Veh versus RGFP966}} = 0.0439$). n.s., not significant, $^{*}P < 0.05$, $^{**}P < 0.01$, $^{***}P < 0.001$.

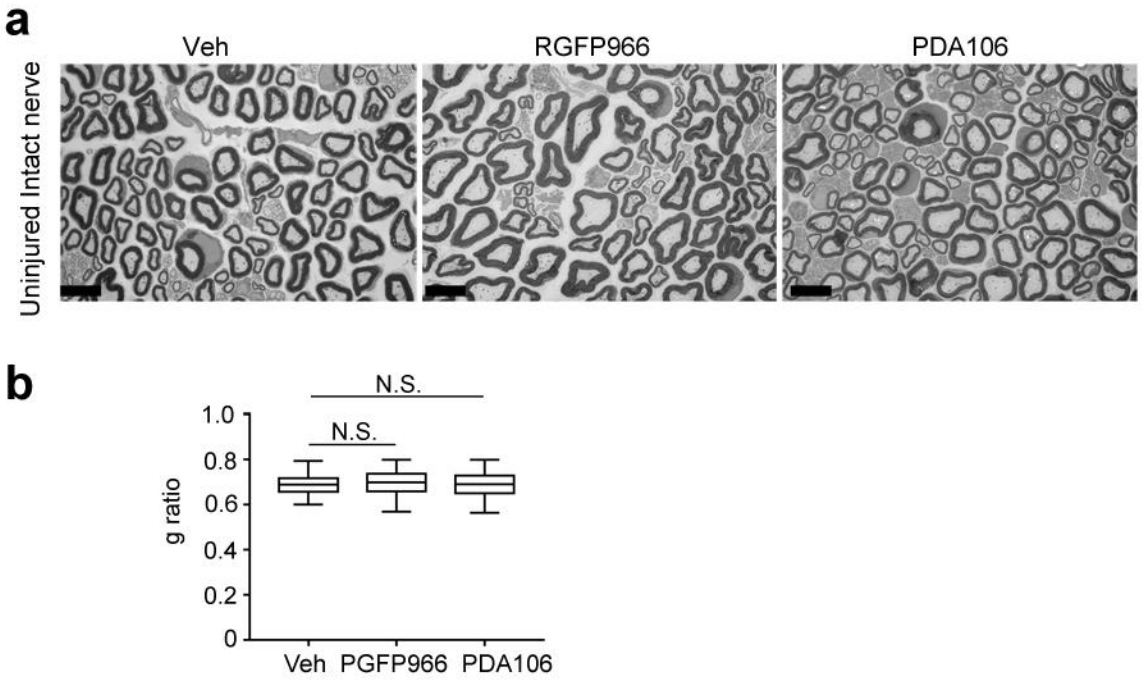

Supplementary Figure 5. Treatment of HDAC3 inhibitors does not affect myelin thickness of the intact sciatic nerves in adult mice. (**a**) Representative electron micrographs of intact sciatic nerves from Veh-, RGFP966-, and PDA106-treated adult mice at Dpi 35. n = 3 animals/group, with 5 images for each mouse. Scale bars: 2 µm. (**b**) Box plots of g ratios of the intact sciatic nerves from Veh-, RGFP966-, and PDA106-treated mice at Dpi 35. (Data are presented as mean ± s.e.m.; n = 203 axons from 3 control mice, 202 axons from 3 RGFP966 treated mice and 200 axons from 3 PDA106 treated mice; Whiskers show the minimum and maximum, boxes extend from the first to the third quartiles with cross lines at the medians; one-way ANOVA with Tukey's multiple comparisons test, $F_{(2, 602)}$ = 2.48, $P_{\text{Veh versus RGFP966}}$ = 0.0679, $P_{\text{Veh versus PDA106}}$ = 0.5701). n.s., not significant.

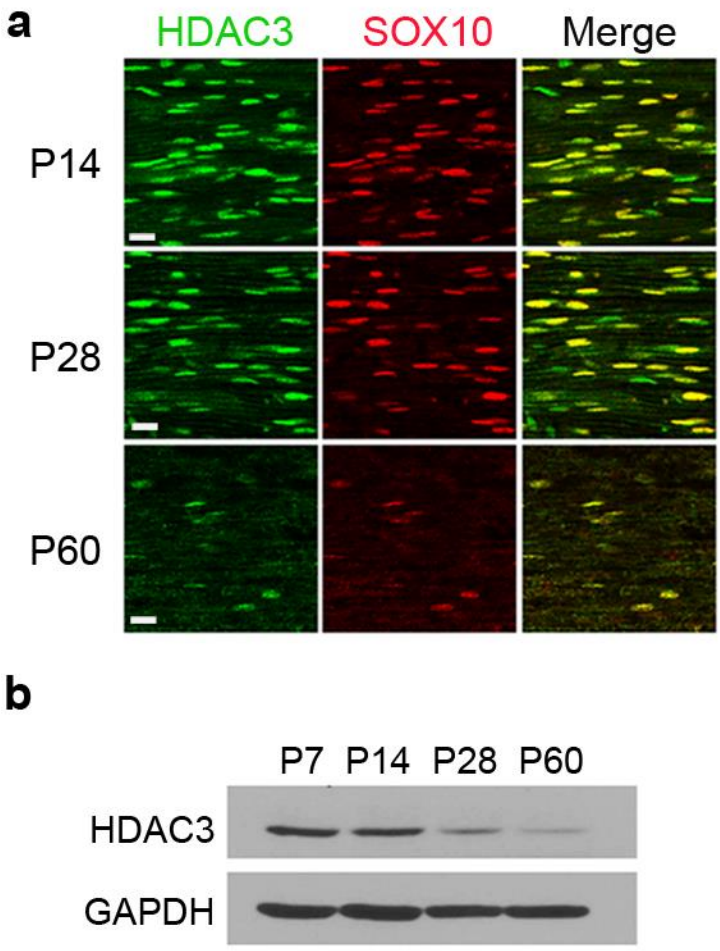

Supplementary Figure 6. HDAC3 expression in sciatic nerves at postnatal and adult stages. (**a**) Immunofluorescence labeling for HDAC3 (green) and SOX10 (red) in sciatic nerves at indicated stages. *n* = 5 animals/group, with 5 images for each mouse. Scale bars: 20 μm. (**b**) Western blots for HDAC3 expression in sciatic nerves at indicated stages. *n* = 3 independent experiments. GAPDH was detected as a loading control.

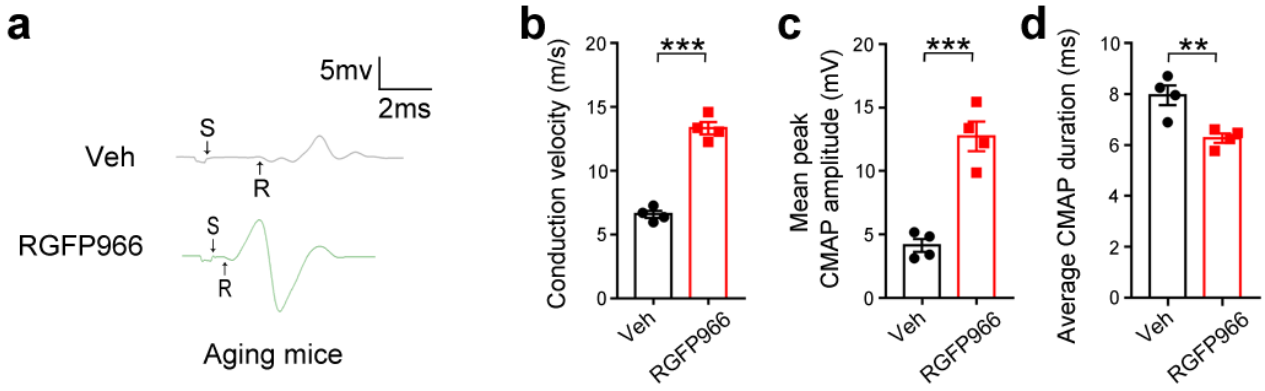

Supplementary Figure 7. HDAC3 inhibitor treatment enhances functional recovery after sciatic nerve transection in aging mice. (**a**) Wildtype aging mice at 10-12 months of age were treated daily for the first week and then every two days until Dpi 14 beginning the day after sciatic nerve transection. Representative recordings of CMAPs of regenerated sciatic nerves at Dpi 35 from Veh- and RGFP966-treated mice (S, stimulus; R, initiation of CMAP response). *n* = 4 animals/group. (**b-d**) Quantification of the conduction velocity (**b**), mean peak of CMAP amplitude (**c**), and average CMAP duration (**d**) of injured sciatic nerves from Veh- and RGFP966-treated mice. (Data are presented as mean ± s.e.m.; *n* = 4 animals/group; two-tailed unpaired Student's *t*-test; b, $P < 0.0001$, $t = 12.11$, d.f. = 6; c, $P = 0.0005$, $t = 6.764$, d.f. = 6; d, $P = 0.0077$, $t = 3.933$, d.f. = 6). $^{**}P < 0.01$, $^{***}P < 0.001$.

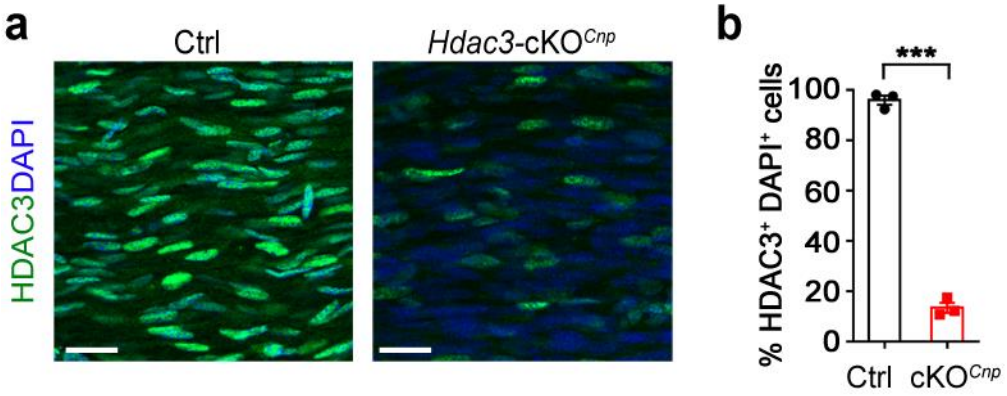

Supplementary Figure 8. Recombination efficiency in the sciatic nerves of *Hdac3*-cKO mice driven by *Cnp*-Cre. (**a**) Representative images of longitudinal cryosections of sciatic nerves from control and *Hdac3*-cKO mice at P8 immunostained for HDAC3 (green) and SOX10 (red). n = 3 animals/group, with 5 images for each mouse. Scale bar, 20 μm. (**b**) Percentage of $HDAC3^+$ cells among DAPI nuclei in control and *Hdac3*-cKO sciatic nerves at P8. (Data are presented as mean ± s.e.m.; n = 3 animals/group; two-tailed unpaired Student's t-test; $P < 0.0001$, $t = 30.28$, d.f. = 4). ***$P < 0.001$.

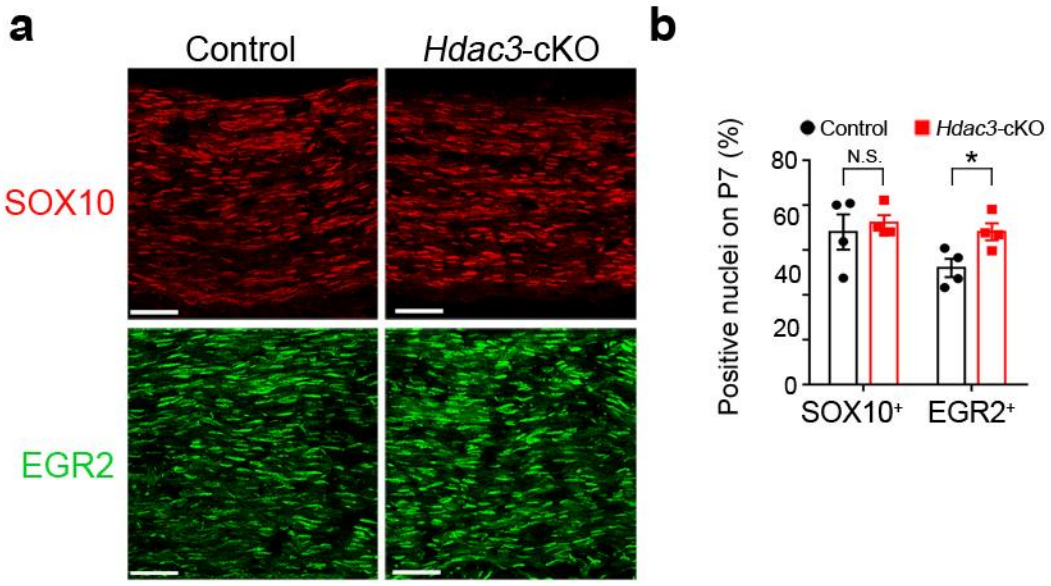

Supplementary Figure 9. Increase of EGR2$^+$ differentiated SCs in HDAC3-deficient sciatic nerves. (**a**) Immunofluorescence labeling for SOX10 (red) and EGR2 (green) in control and *Hdac3*-iKO sciatic nerves at P7. n = 4 animals/group, with 5 images for each mouse. Scale bars: 50 µm. (**b**) Percentage of SOX10$^+$ and EGR2$^+$ SCs among DAPI nuclei in control and *Hdac3*-iKO sciatic nerves at P7. (Data are presented as mean ± s.e.m.; n = 4 animals/group; two-tailed unpaired Student's t-test; SOX10, P = 0.6492, t = 0.4786, d.f. = 6; EGR2, P = 0.0276, t = 2.894, d.f. = 6). n.s., not significant, *P < 0.05.

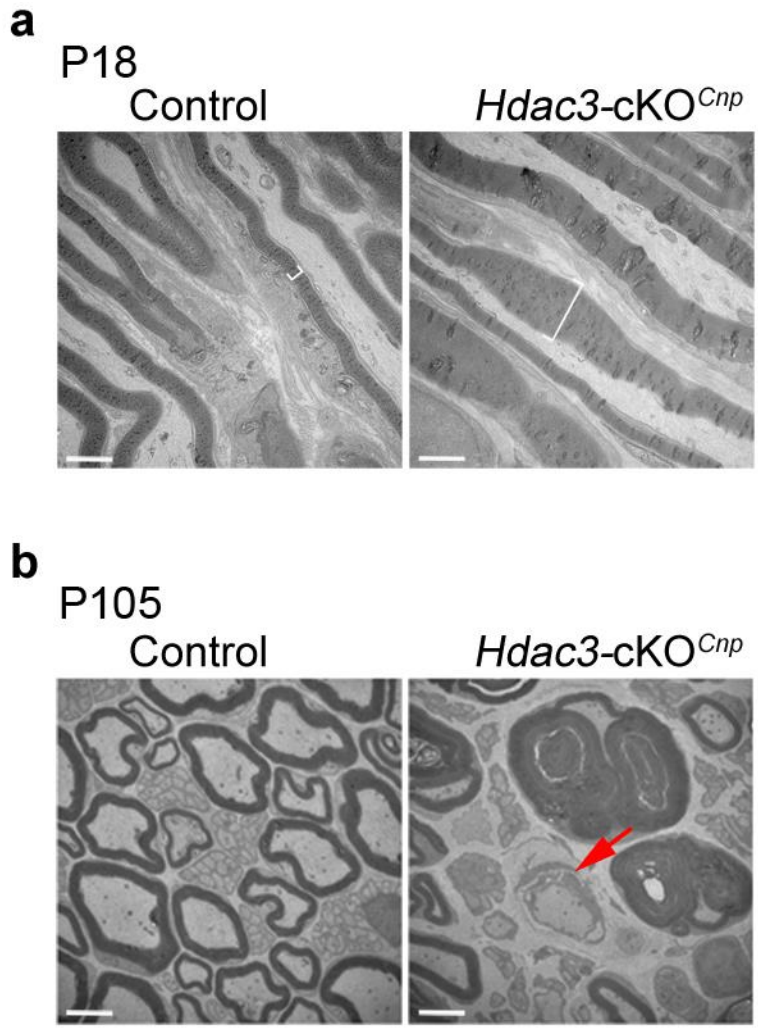

Supplementary Figure 10. *Hdac3*-deficient mice develop hypermyelination at P18 and progressive demyelination at adult stage in peripheral nerves. (**a**) Representative electron micrographs of longitudinal sections of sciatic nerves from control and *Hdac3*-cKO mice at P18. The brackets indicate the thickness of myelin sheath. n = 4 animals/group, with 5 images for each mouse. Scale bars: 2 μm. (**b**) Representative electron micrographs of cross sections of sciatic nerves of control and *Hdac3*-cKO mice at P105. Arrow indicates a demyelinated axon. n = 4 animals/group, with 5 images for each mouse. Scale bars: 2 μm.

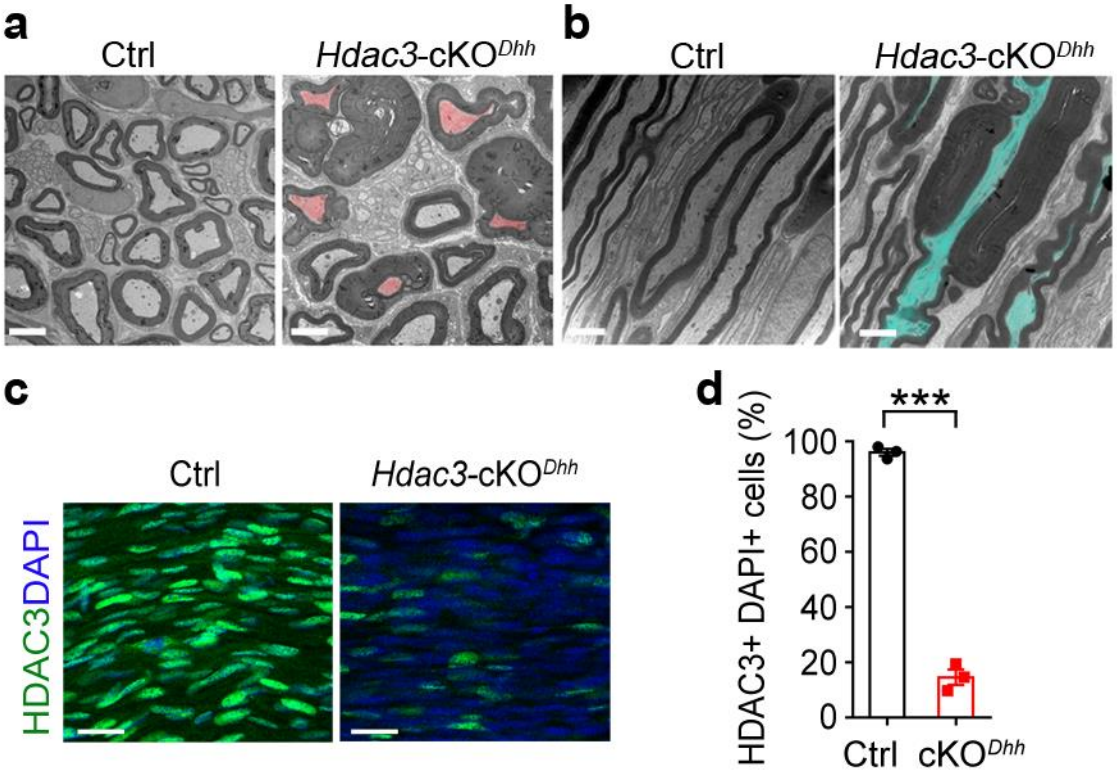

Supplementary Figure 11. Mice with *Hdac3* ablation in *Dhh*-Cre-expressing SCs exhibit hypermyelination. (**a,b**) Electron micrographs of (**a**) cross sections and (**b**) longitudinal sections of sciatic nerves from control (*Hdac3*$^{fl/fl}$) and *Hdac3*-cKO (*Hdac3*$^{fl/fl}$*; Dhh-Cre*$^{+/-}$) mice at P28. Colored regions mark axons. *n* = 3 animals/group, with 5 images for each mouse. Scale bars: 2 μm. (**c**) Representative images of longitudinal cryosections of sciatic nerves from control and *Hdac3*-cKO mice at P8 immunostained for HDAC3 (green) and SOX10 (red). *n* = 3 animals/group, with 5 images for each mouse. Scale bar, 20 μm. (**d**) Percentage of HDAC3^{+} cells among DAPI nuclei in control and *Hdac3*-cKO sciatic nerves at P8. (Data are presented as mean ± s.e.m.; *n* = 3 animals/group; two-tailed unpaired Student's *t*-test; $P < 0.0001$, $t = 26.71$, d.f. = 4). ***$P < 0.001$.

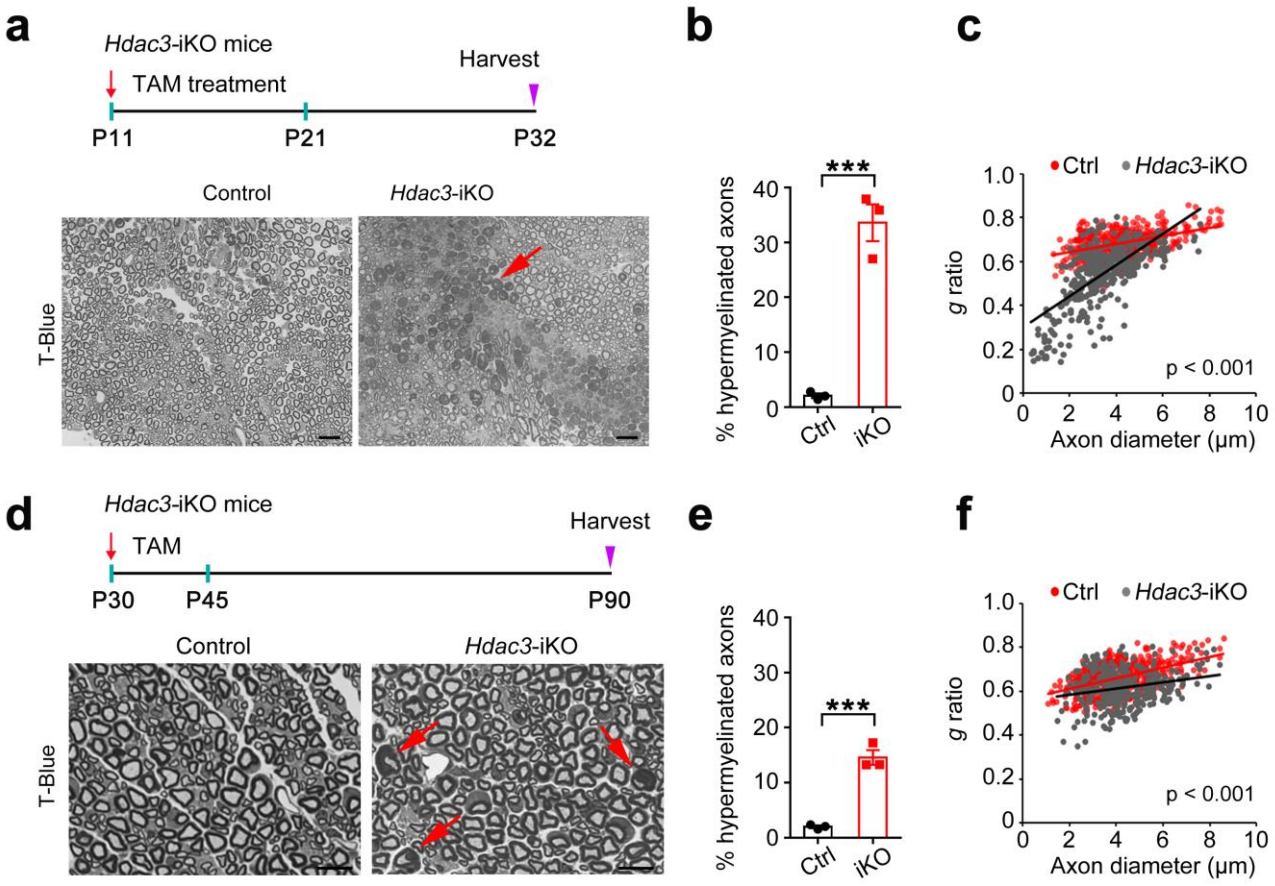

Supplementary Figure 12. Inducible deletion of *Hdac3* at different stages leads to hypermyelination. (**a**) Upper: Schematic diagram showing tamoxifen treatment scheme. Mice were treated with tamoxifen from P11 to P21 and sciatic nerves were harvested at P32. Bottom: Representative toluidine blue-stained images of semi-thin cross-sections of sciatic nerves from control and *Hdac3*-iKO mice. n = 3 animals/group, with 5 images for each mouse. Scale bars: 20 μm. (**b**) Quantification of hypermyelinated axons at P32 from control and *Hdac3*-iKO mice. (Data are presented as mean ± s.e.m.; n = 3 animals/group; two-tailed unpaired Student's t-test; P = 0.0007, t = 9.342, d.f. = 4). (**c**) Quantification of g ratios of axons at P32 from control and *Hdac3*-iKO mice. (Data are presented as mean ± s.e.m.; n = 415 axons from 3 control mice and 392 axons from 3 iKO mice; two-tailed unpaired Student's t-test; $P < 0.0001$, t = 18.95, d.f. = 805). (**d**) Upper: Schematic diagram showing tamoxifen treatment scheme. Mice were treated with tamoxifen from P30 to P45 and sciatic nerves were harvested at P90. Bottom: Representative toluidine blue-stained images of semi-thin cross-sections of sciatic nerves from control and *Hdac3*-iKO mice. n = 3 animals/group, with 5 images for each mouse. Scale bars: 20 μm. (**e**) Quantification of hypermyelinated axons at P90 from control and *Hdac3*-iKO mice. (Data are presented as mean ± s.e.m.; n = 3 animals/group; two-tailed unpaired Student's t-test; P = 0.0007, t = 9.373, d.f. = 4). (**f**) Quantification of g ratios of axons at P90 from control and *Hdac3*-iKO mice. (Data are presented as mean ± s.e.m.; n = 426 axons from 3 control mice and 351 axons from 3 iKO mice two-tailed unpaired Student's t-test; $P < 0.0001$, t = 8.498, d.f. = 775). ***$P < 0.001$.

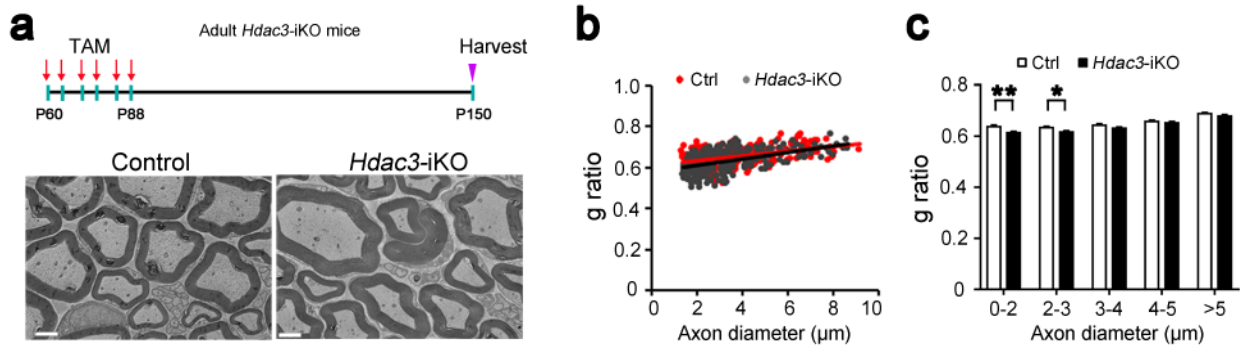

Supplementary Figure 13. Effect of *Hdac3* ablation in adult mice on peripheral myelination. (**a**) Upper: A diagram of tamoxifen administration scheme. Adult control and *Hdac3*-iKO mice were treated with tamoxifen from P60 to P64, from P72 to P76, and from P84 to 88. Sciatic nerves were harvested at P150. Bottom: Representative electron micrographs of cross sections of sciatic nerves from control and *Hdac3*-iKO mice at P150. n = 3 animals/group, with 5 images for each mouse. Scale bars: 2 μm. (**b**) Dot plot of g ratios of axons at P150 from control and *Hdac3*-iKO mice (n = 3 animals/group). (**c**) Quantification of g ratios of groups of axons with the indicated diameters at P150. (Data are presented as mean ± s.e.m.; n = 3 animals/group; two-tailed unpaired Student's t-test; 0 -2 μm, P = 0.0041, t = 2.934, d.f. = 112; 2 -3 μm, P = 0.0148, t = 2.461, d.f. = 182). *P < 0.05, **P < 0.01.

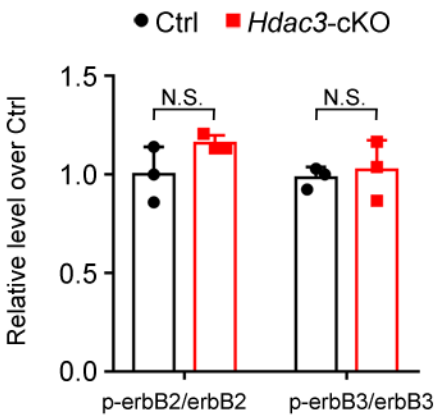

Supplementary Figure 14. NRG1 receptor erbB2/3 activity is comparable between control and *Hdac3*-cKO sciatic nerves. Quantification of the ratio between p-erbB2/3 and erbB2/3 analyzed by western blot analysis of control and *Hdac3*-cKO sciatic nerves at P13 (Data are presented as mean ± s.e.m.; n = 3 animals/group; two-tailed unpaired Student's t-test). n.s., not significant.

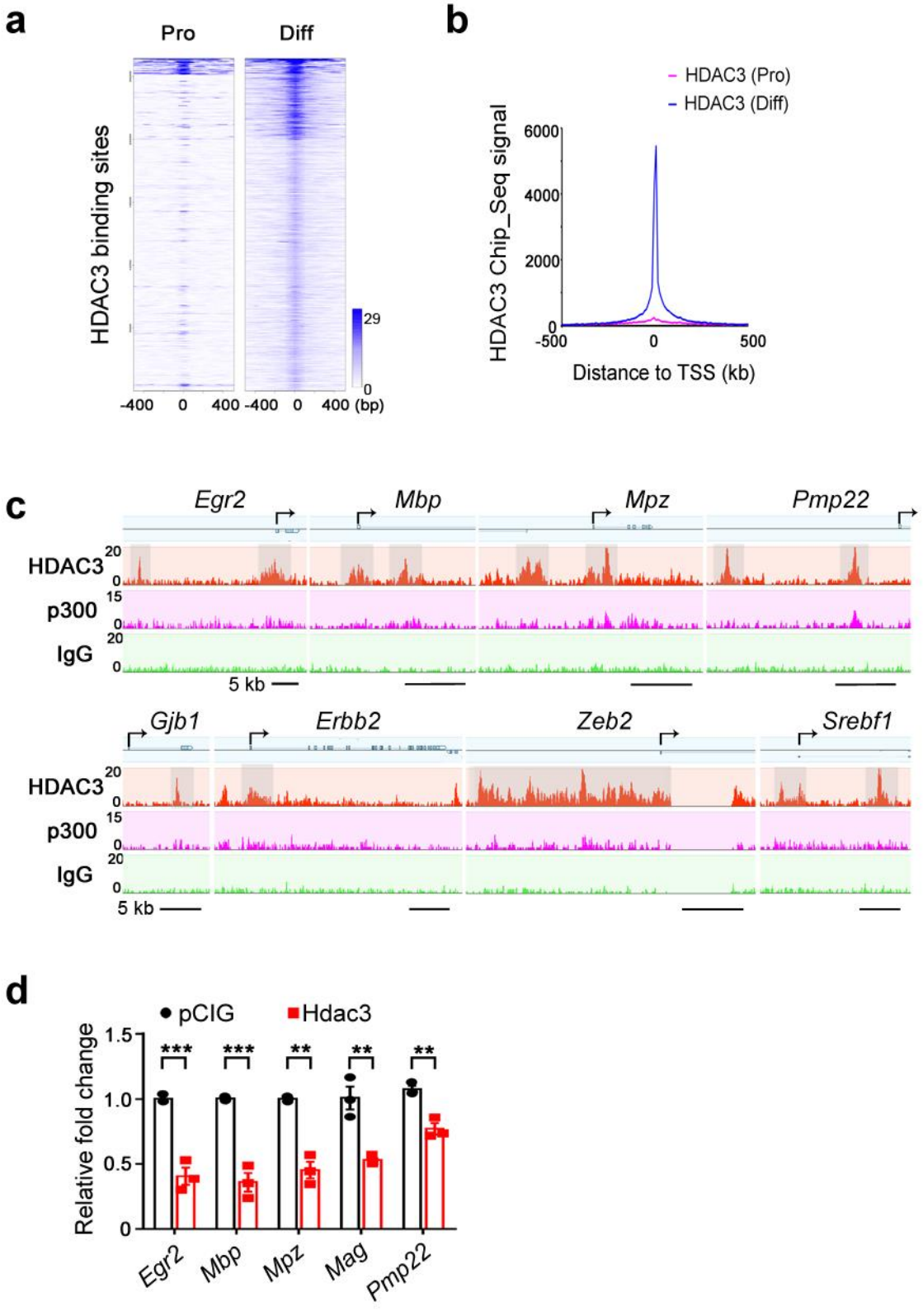
a
Pro
Diff
HDAC3 binding sites
29
0
-400 0 400 -400 0 400 (bp)
b
HDAC3 (Pro)
HDAC3 (Diff)
HDAC3 Chip_Seq signal
6000
4000
2000
0
-500 0 500
Distance to TSS (kb)
c
Egr2
Mbp
Mpz
Pmp22
HDAC3
p300
IgG
5 kb
Gjb1
Erbb2
Zeb2
Srebf1
HDAC3
p300
IgG
5 kb
d
pCIG
Hdac3
Relative fold change
1.5
1.0
0.5
0
***
***
**
**
**
Egr2
Mbp
Mpz
Mag
Pmp22

Supplementary Figure 15. HDAC3 directly targets and represses expression of myelin-associated genes. (**a**) Heatmaps of HDAC3-binding signals obtained by ChIP-seq in SCs under proliferation (Pro) and differentiation (Diff) conditions. Each line on y axis represents a genomic region ±0.4 kb flanking HDAC3 summits. (**b**) The distribution pattern of HDAC3-binding signals in SCs under proliferation (Pro) and differentiation (Diff) conditions mapped to the transcription start site (TSS) of their closest Ensembl annotated genes. (**c**) Representative ChIP-seq signals of myelin-associated genes (upper panel) and pro-myelinating transcriptional regulators (lower panel) that are targeted by HDAC3 but not p300. $n = 2$ independent experiments with similar results. (**d**) q-PCR showing expression of myelination-related genes in SCs that express control GFP-expressing pCIG and *Hdac3*-expressing vectors. (Data are presented as mean ± s.e.m.; $n = 3$ independent experiments; two-tailed unpaired Student's *t*-test; *Egr2*, $P = 0.00097$, $t = 8.679$, d.f. = 4; *Mbp*, $P = 0.0009$, $t = 8.93$, d.f. = 4; *Mpz*, $P = 0.0011$, $t = 8.329$, d.f. = 4; *Mag*, $P = 0.0062$, $t = 5.268$, d.f. = 4; *Pmp22*, $P = 0.004$, $t = 5.925$, d.f. = 4). $^{**}P < 0.01$, $^{***}P < 0.001$.

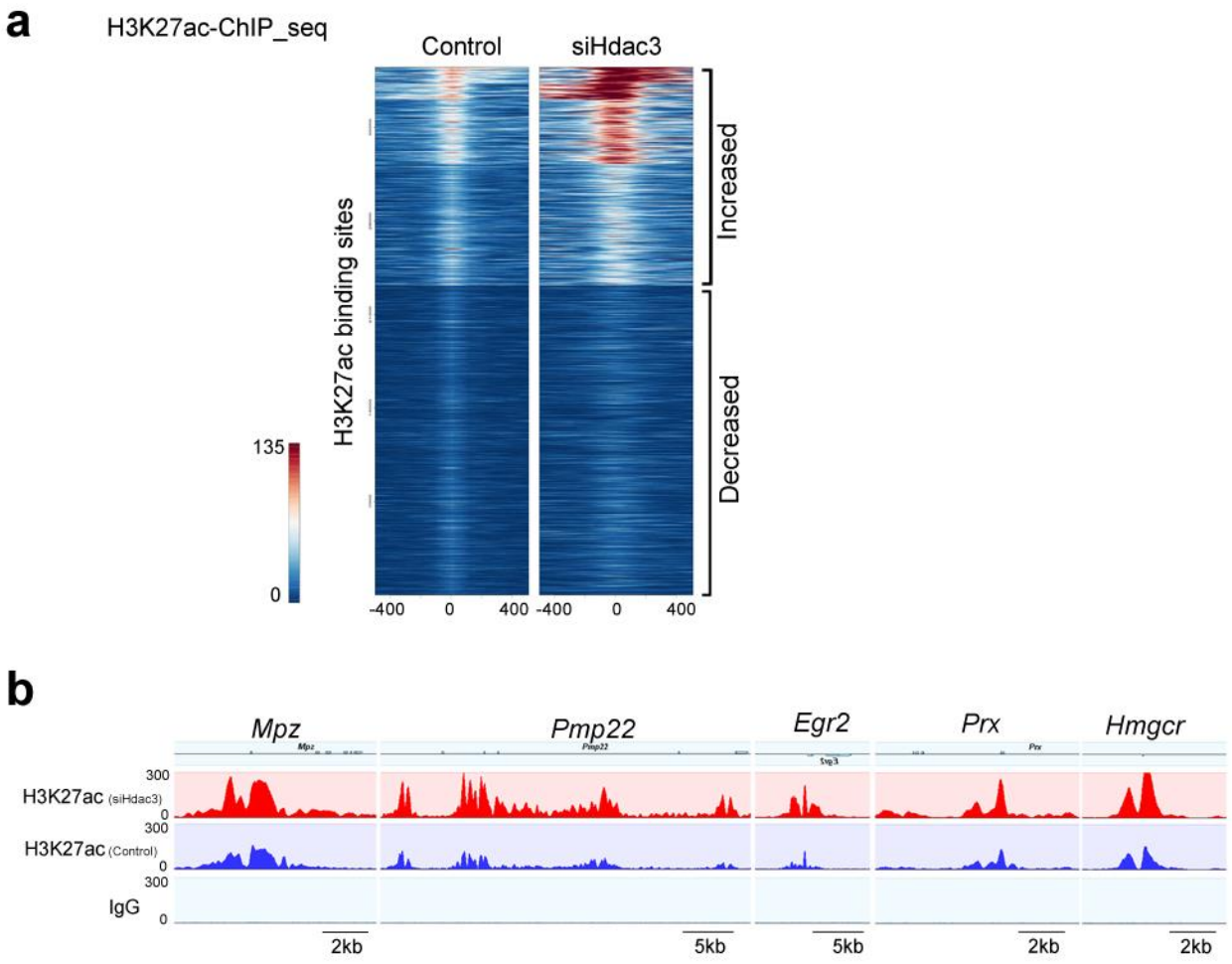

Supplementary Figure 16. Knockdown of HDAC3 elevates H3K27ac signals in the regulatory elements of myelination-associated genes in SCs. (**a**) Heatmaps of H3K27ac signals obtained by ChIP-seq in mock control or si*Hdac3* transfected SCs. Each line on y axis represents a genomic region ± 400 bp flanking H3K27ac summits in control SCs. (**b**) Genome browser view of the distribution of H3K27ac signals on the myelination-associated *Mpz*, *Pmp22*, *Egr2*, *Prx* and *Hmgcr* gene loci. Note that an increase in H3K27ac signals in the enhancer/promoter elements in SCs transfected with *Hdac3* siRNA. The ChIP-seq experiments were performed once using a pool of control or si*Hdac3* transfected SCs (10 petri dishes per group).

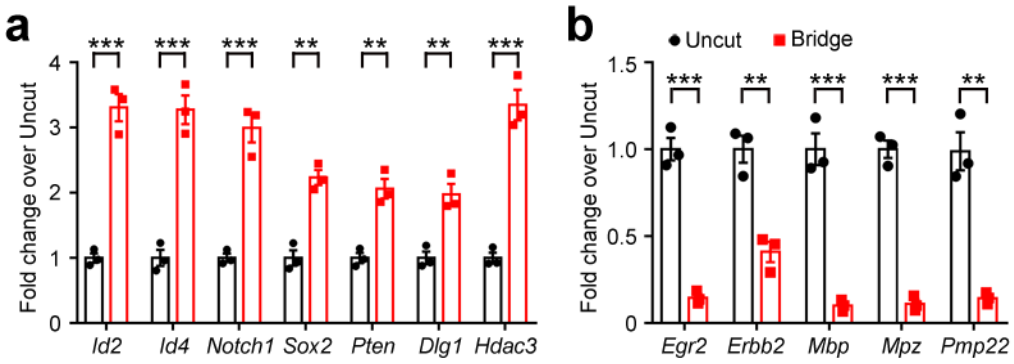

Supplementary Figure 17. Expression of myelination-related genes in the regenerating sites in sciatic nerves. (**a,b**) q-PCR analysis of expression of myelination-inhibitory genes (**a**) and myelination-associated genes (**b**) in the regenerating sites of sciatic nerves at Dpi 14. (Data are presented as mean ± s.e.m.; n = 3 independent experiments (uncut nerves and bridge tissues from 3 animals/experiment); two-tailed unpaired Student's t-test; a, *Id2*, P = 0.0005, t = 10.44, d.f. = 4; *Id4*, P = 0.0008, t = 9.051, d.f. = 4; *Notch1*, P = 0.00098, t = 8.656, d.f. = 4; *Sox2*, P = 0.0017, t = 7.528, d.f. = 4; *Pten*, P = 0.0032, t = 6.309, d.f. = 4; *Dlg1*, P = 0.0066, t = 5.185, d.f. = 4; *Hdac3*, P = 0.0008, t = 9.522, d.f. = 4; b, *Egr2*, P = 0.0002, t = 15.28, d.f. = 4; *Erbb2*, P = 0.0038, t = 6.045, d.f. = 4; *Mbp*, P = 0.0006, t = 9.641, d.f. = 4; *Mpz*, P < 0.0001, t = 15.95, d.f. = 4; *Pmp22*, P = 0.0016, t = 7.607, d.f. = 4). **P < 0.01, ***P < 0.001.

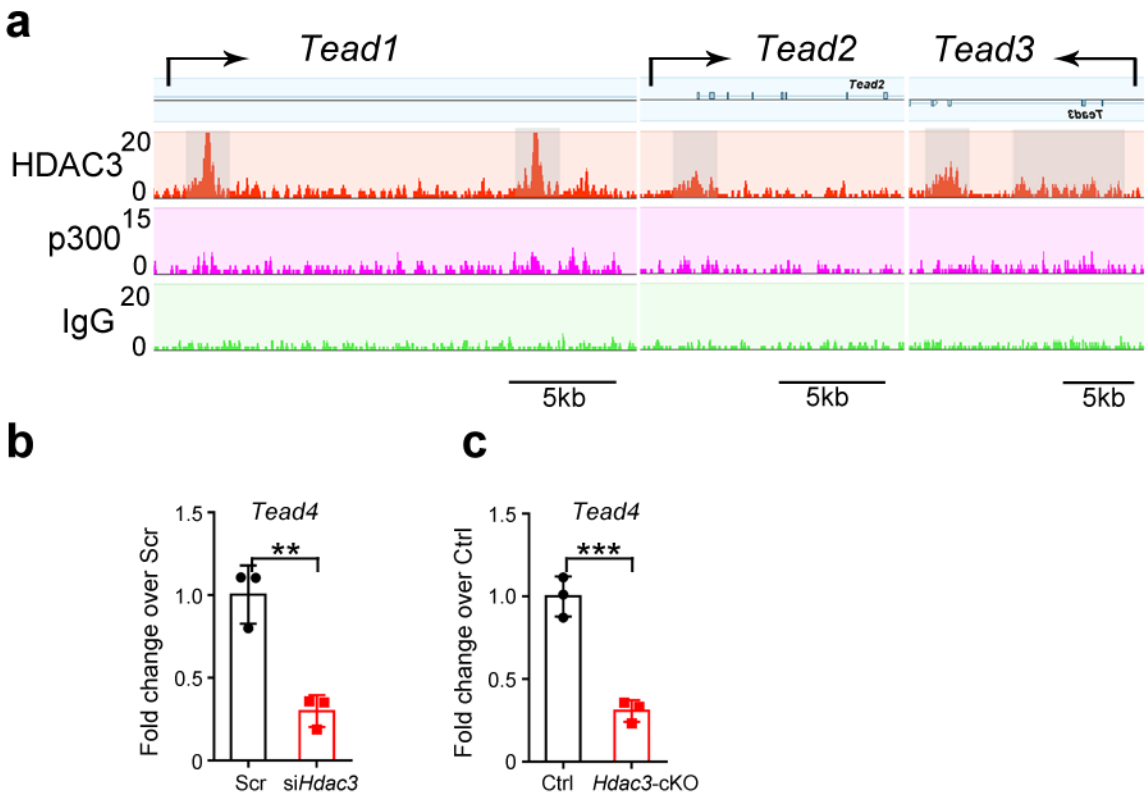

Supplementary Figure 18. HDAC3 and p300 genomic occupancy on the gene loci of TEAD family members. (**a**) Genome browser view of the distribution of HDAC3 and p300 signals on the *Tead1*, *Tead2*, and *Tead3* loci. Note that HDAC3 binding was mainly detected in these gene loci. *n* = 2 independent experiments with similar results. (**b,c**) qRT-PCR analyses of *Tead4* expression in si*Hdac3*-treated SCs (**b**) or sciatic nerves of *Hdac3*-cKO mice (**c**). (Data are presented as mean ± s.e.m.; n = 3 independent experiments; two-tailed unpaired Student's t-test; b, $P = 0.0037$, $t = 6.083$, d.f. = 4; c, $P = 0.001$, $t = 8.707$, d.f. = 4). $^{**}P < 0.01$, $^{***}P < 0.001$.

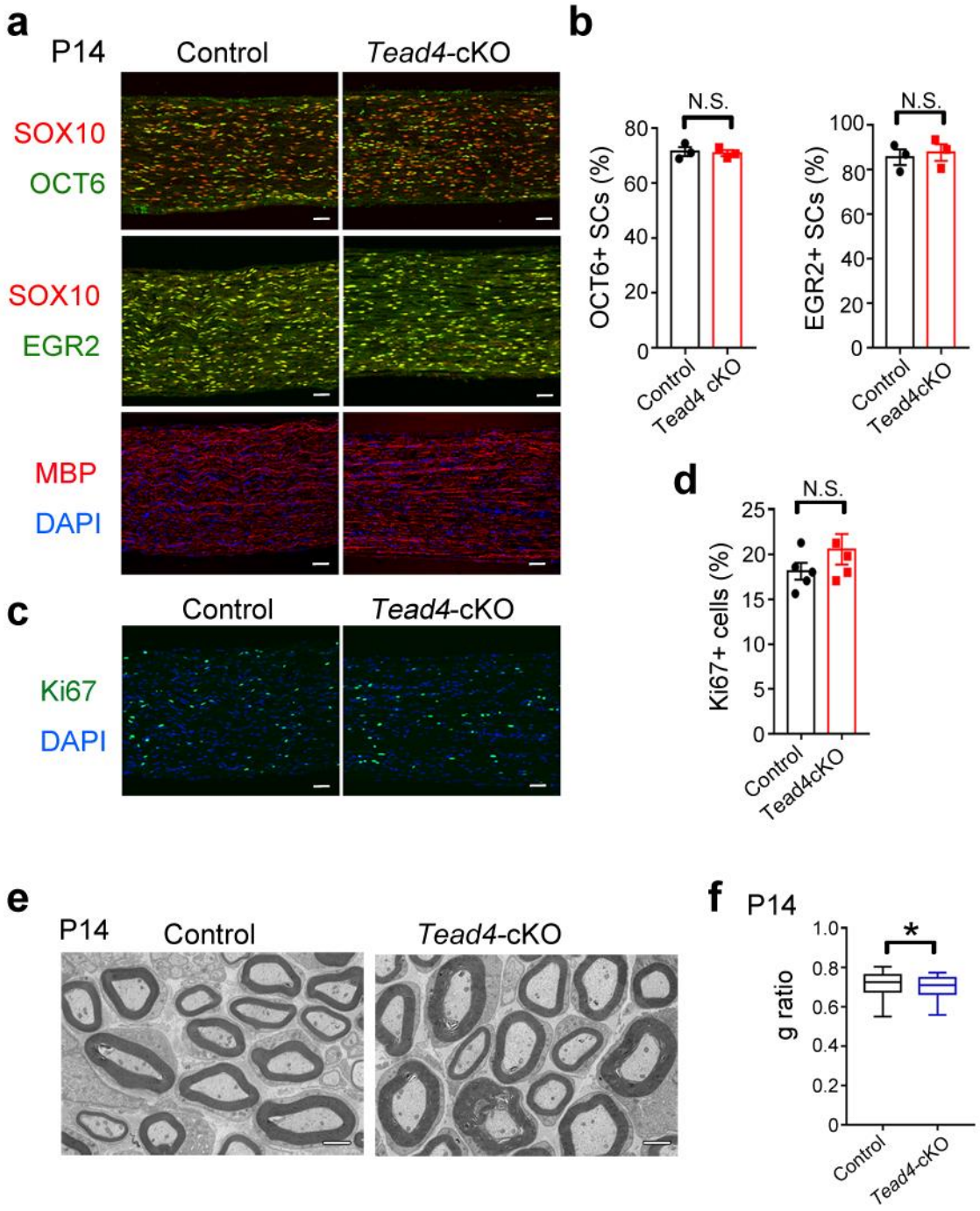

Supplementary Figure 19. Myelination in *Tead4*-cKO mice at early postnatal stages. (**a**) Longitudinal sections of sciatic nerves from *Tead4*-cKO and control mice at P14 were immunostained with SOX10, OCT6, EGR2, and MBP. n = 3 animals/group, with 5 images for each mouse. Scale bars: 50 μm. (**b**) Quantification of $OCT6^+$ and $EGR2^+$ SCs among $SOX10^+$ SCs in P14 control and *Tead4*-cKO sciatic nerves. (Data are presented as mean ± s.e.m.; n = 3 animals/group; two-tailed unpaired Student's t-test; OCT6, P = 0.7902, t = 0.2844, d.f. = 4; EGR2, P = 0.7019, t = 0.4113, d.f. = 4). (**c**) Immunofluorescence labeling for Ki67 (green) in P14 sciatic nerves from control and *Tead4*-cKO nerves. DAPI (blue) was used to stain nuclei. n = 3

animals/group, with 5 images for each mouse. Scale bars: 50 μm. (**d**) Quantification of $Ki67^+$ SCs in P14 control and *Tead4*-cKO sciatic nerves. (Data are presented as mean ± s.e.m.; n = 3 animals/group; two-tailed unpaired Student's t-test; P = 0.2425, t = 1.262, d.f. = 8). (**e**) Electron microscopy analysis of cross sections of control and *Tead4*-cKO sciatic nerves at P14. n = 3 animals/group, with 5 images for each mouse. Scale bars: 2 μm. (**f**) Quantification of g ratios at P14 from control and *Tead4*-cKO sciatic nerves. (Data are presented as mean ± s.e.m.; n = 161 axons from 3 control mice and 133 axons from 3 cKO mice; Whiskers show the minimum and maximum, boxes extend from the first to the third quartiles with cross lines at the medians; two-tailed unpaired Student's t-test; P = 0.0103, t = 2.581, d.f. = 292). n.s., not significant, *P < 0.05.

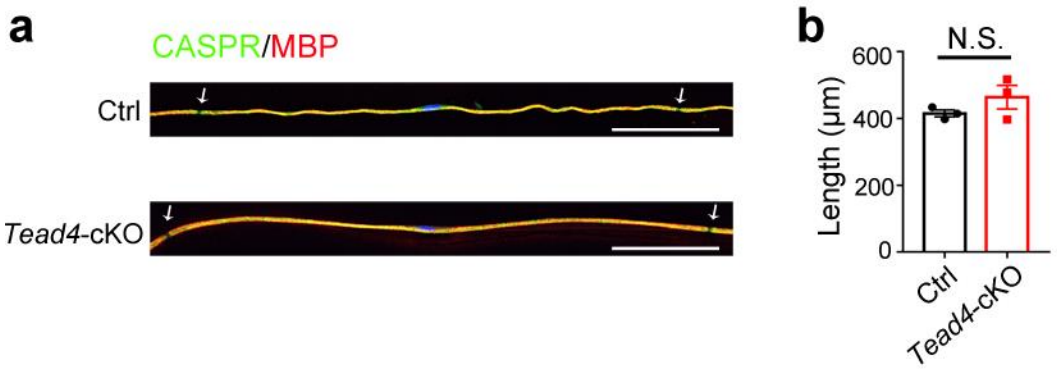

Supplementary Figure 20. Ablation of *Tead4* exerts no significant effect on myelin elongation. (**a**) Representative images of teased fibers of sciatic nerves from control and *Tead4*-cKO mice at P14 immunostained for MBP (red), CASPR (green) to visualize nodes of Ranvier by staining paranodes), and DAPI (blue). Arrows indicate the location of the nodes. n = 3 animals/group, with 5 images for each mouse. Scale bar, 100 μm. (**b**) Quantification of internode lengths of teased fibers from sciatic nerves of Ctrl or *Tead4*-cKO mice. (Data are presented as mean ± s.e.m.; n = 3 animals/group; two-tailed unpaired Student's t-test; P = 0.2576, t = 1.319, d.f. = 4). n.s., not significant.

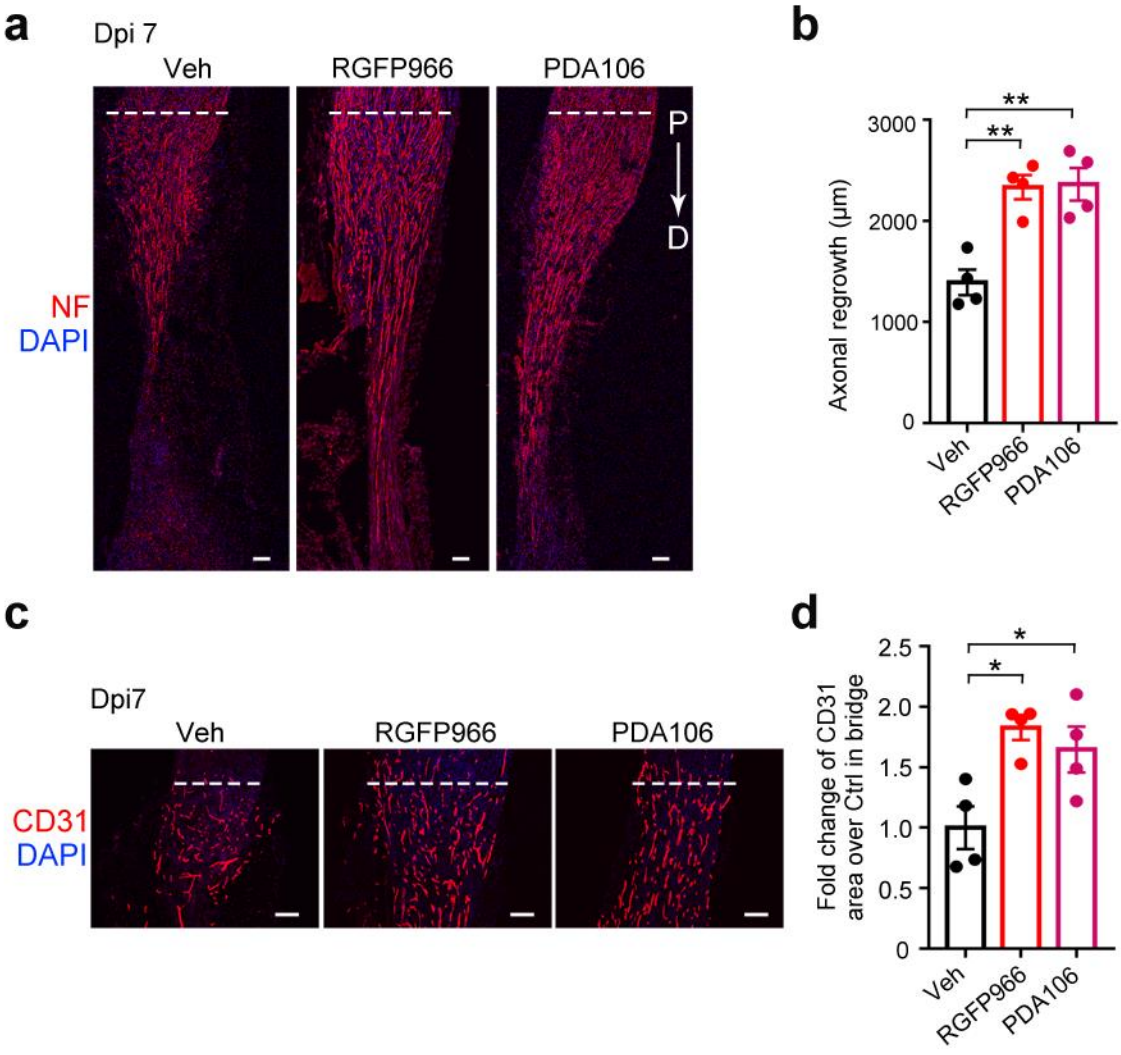

Supplementary Figure 21. Effects of HDAC3 inhibition on axon regrowth and blood vessel formation. (**a**) Representative images of longitudinal cryosections of tissue bridges (regions under the dashes lines) from injured sciatic nerves after indicated treatment at Dpi 7 immunostained for neurofilament M (NF; red) and counterstained with DAPI (blue). P: proximal; D: distal. n = 4 animals/group. Scale bars, 100 μm. (**b**) Quantification of regenerating axons at different distances caudal to the lesion sites. (Data are presented as mean ± s.e.m.; n = 4 animals/group; One-way ANOVA with Tukey's multiple comparisons test; $F_{(2, 9)}$ = 16.22, $P_{\text{Veh versus RGFP966}}$ = 0.0023, $P_{\text{Veh versus PDA106}}$ = 0.0019). (**c**) Representative images of longitudinal cryosections of tissue bridges (regions under the dashes lines) from injured sciatic nerves after indicated treatment at Dpi 7 immunostained for CD31 (red) and counterstained with DAPI (blue). n = 3 animals/group. Scale bar, 100 μm. (**d**) Quantification of $CD31^+$ area within the bridge. (Data are presented as mean ± s.e.m.; n = 4 animals/group; One way ANOVA with Tukey's multiple comparisons test; $F_{(2, 9)}$ = 6.579, $P_{\text{Veh versus RGFP966}}$ = 0.0171, $P_{\text{Veh versus PDA106}}$ = 0.0452). *P < 0.05; **P < 0.01.

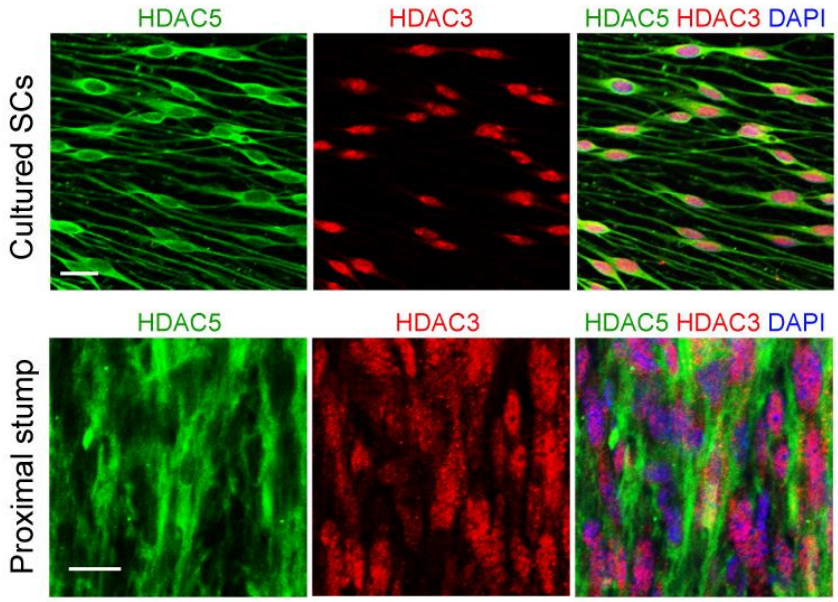

Supplementary Figure 22. Expression of HDAC5 and HDAC3 in SC and injured sciatic nerves. Representative images of cultured rat SCs (upper) and tissue bridges in injured sciatic nerves at Dpi 6 (low) was immunostained with HDAC5 (green), HDAC3 (red) and DAPI (blue). Results are representative of 5 independent experiments, with 5 images for each experiment. Scale bar: 20 μm.

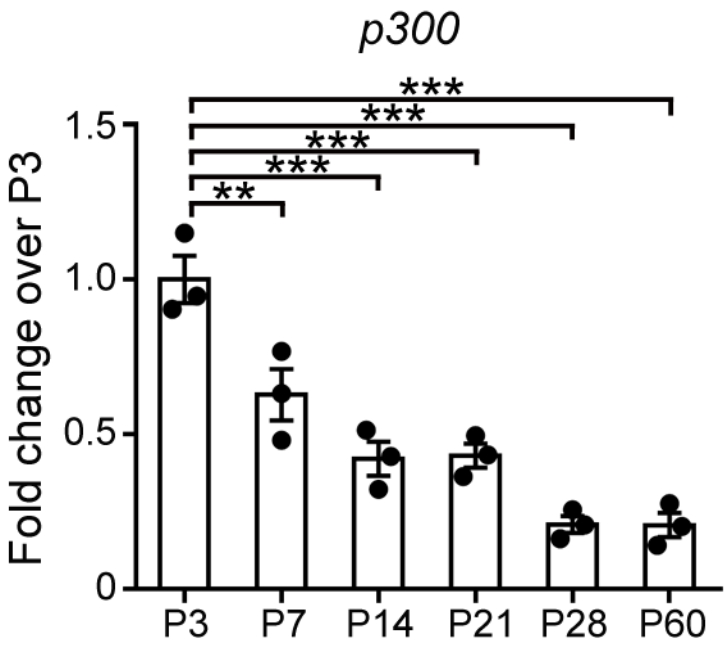

Supplementary Figure 23. p300 expression pattern during peripheral nerve development. qPCR quantification of *p300* expression in murine sciatic nerve at different stages. (Data are presented as mean ± s.e.m.; $n = 3$ animals/group; One way ANOVA with Tukey's multiple comparisons test; $F_{(5, 12)} = 27.65$, $P_{\text{P3 versus P7}} = 0.0058$, $P_{\text{P3 versus P14}} = 0.0001$, $P_{\text{P3 versus P21}} = 0.0001$, $P_{\text{P3 versus P28}} < 0.0001$, $P_{\text{P3 versus P60}} < 0.0001$). $^{**}P < 0.01$, $^{***}P < 0.001$.

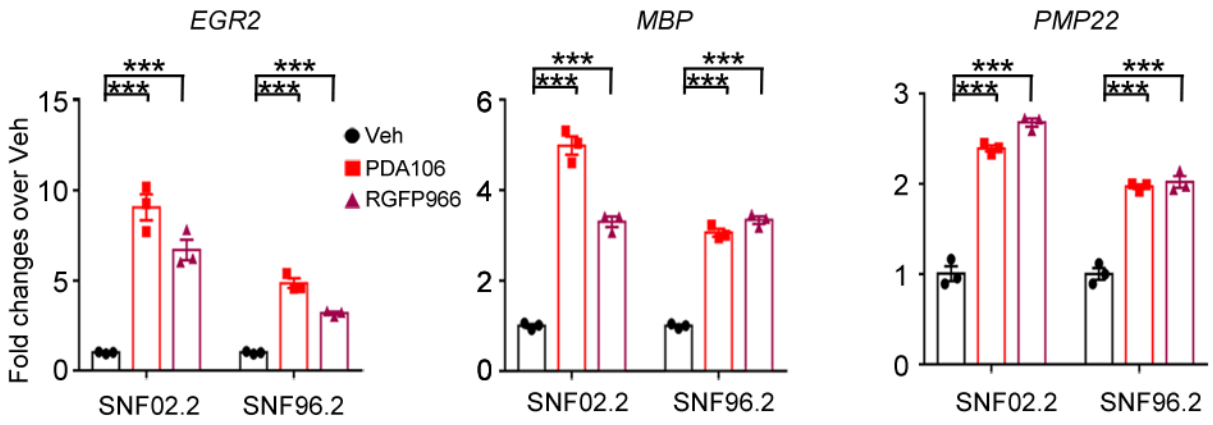

Supplementary Figure 24. Upregulation of myelin gene expression in human SC lines treated with HDAC3 inhibitors. Transcript levels of the myelination-associated genes *EGR2*, *MBP* and *PMP22*, assayed by qRT-PCR, in human neurofibroma-derived Schwann cell lines SNF02.2 and SNF96.2 treated with the HDAC3 inhibitors PDA106 and RGFP966, were normalized to those in Vehicle-treated cells. (Data are presented as mean ± s.e.m.; n = 3 independent experiments; one-way ANOVA with Tukey's multiple comparisons test; *EGR2*, SNF02.2, $F_{(2, 6)} = 61.27$, $P_{\text{Veh versus PDA106}} < 0.0001$, $P_{\text{Veh versus RGFP966}} = 0.0007$; SNF96.2, $F_{(2, 6)} = 138.7$, $P_{\text{Veh versus PDA106}} < 0.0001$, $P_{\text{Veh versus RGFP966}} = 0.0002$; *MBP*, SNF02.2, $F_{(2, 6)} = 212.4$, $P_{\text{Veh versus PDA106}} < 0.0001$, $P_{\text{Veh versus RGFP966}} < 0.0001$; SNF96.2, $F_{(2, 6)} = 318.1$, $P_{\text{Veh versus PDA106}} < 0.0001$, $P_{\text{Veh versus RGFP966}} < 0.0001$; *PMP22*, SNF02.2, $F_{(2, 6)} = 242$, $P_{\text{Veh versus PDA106}} < 0.0001$, $P_{\text{Veh versus RGFP966}} < 0.0001$; SNF96.2, $F_{(2, 6)} = 108.9$, $P_{\text{Veh versus PDA106}} < 0.0001$, $P_{\text{Veh versus RGFP966}} < 0.0001$). ***$P < 0.001$.

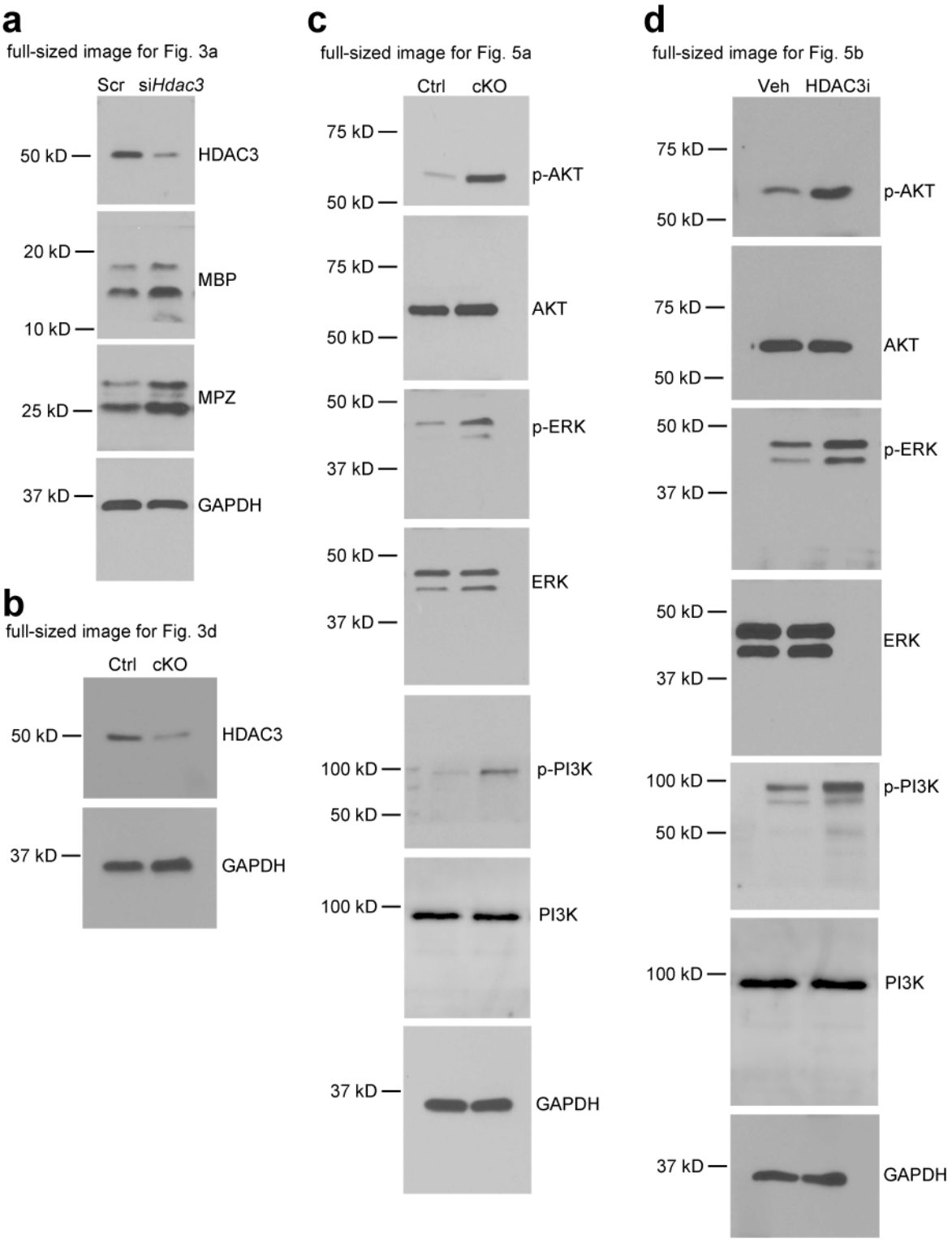

Supplementary Figure 25. Raw gel images for Figures 3a, d and 5a, b.

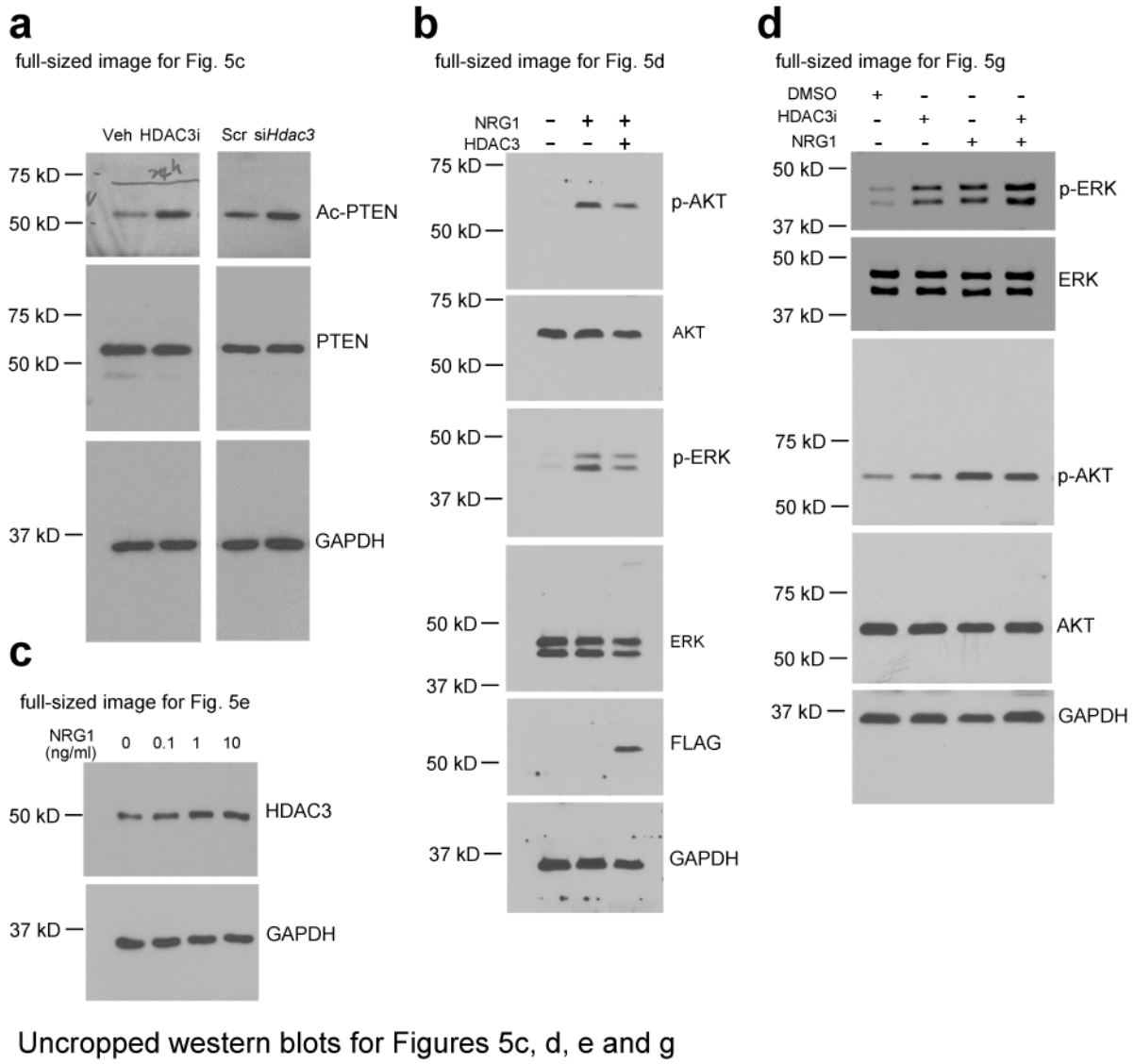

Supplementary Figure 26. Raw gel images for Figures 5c, d, e and g.

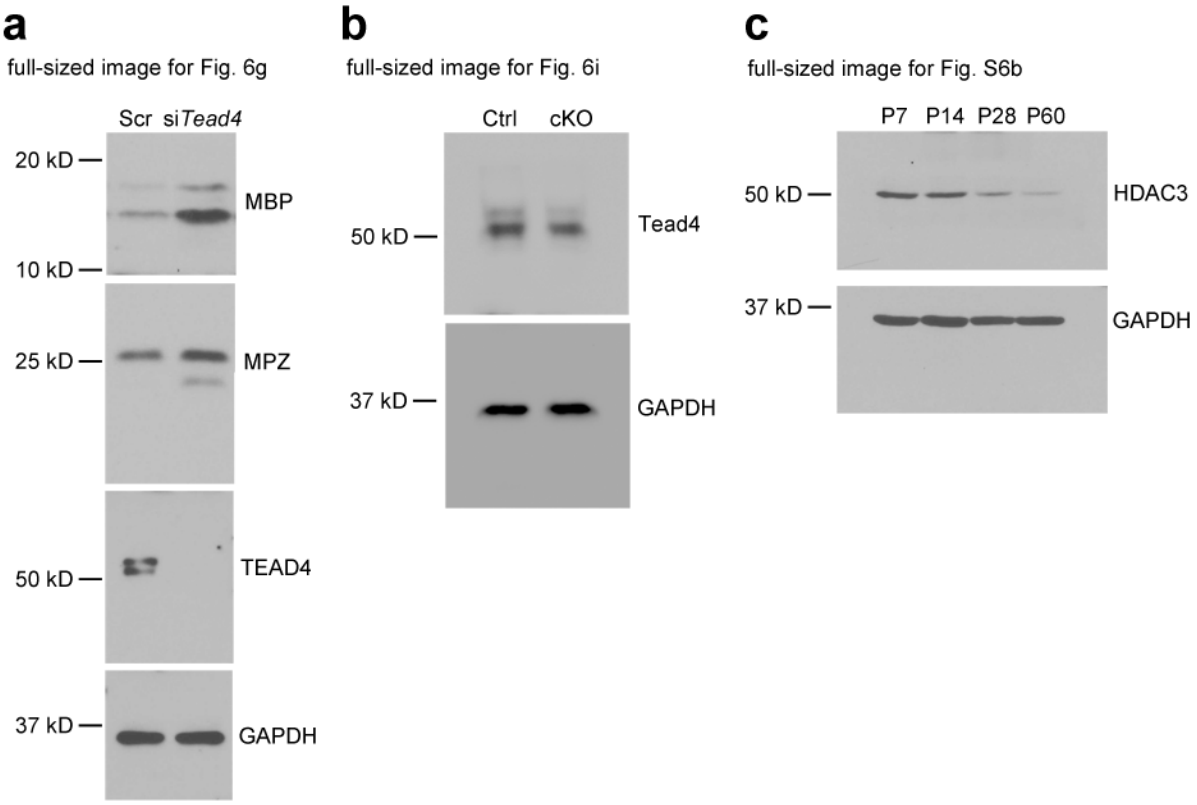

Supplementary Figure 27. Raw gel images for Figures 6g, i and Supplemental Figure 6b.